Spectroscopic gamma camera for use in high dose environments

Yuichiro Ueno[a], Isao Takahashi[a], Takafumi Ishitsu[a], Takahiro Tadokoro[a], Koichi Okada[a], Yasushi Nagumo[a], Yasutake Fujishima[b], Yutaka Kometani[b], Yasuhiko Suzuki[c], Kikuo Umegaki[d]

[a] Research and Development Group, Hitachi, Ltd., Hitachi-shi, Ibaraki-ken, 319-1221 Japan.

[b] Hitachi Works, Hitachi-GE Nuclear Energy, Ltd., Hitachi-shi, Ibaraki-ken, Japan.

[c] Measuring Systems Engineering Dept., Hitachi Aloka Medical, Ltd., Ome-shi, Tokyo, Japan.

[d] Faculty of Engineering, Hokkaido University, Sapporo-shi, Hokkaido, Japan.

E-mail: yuichiro.ueno.bv@hitachi.com

Abstract

We developed a pinhole gamma camera to measure distributions of radioactive material contaminants and to identify radionuclides in extraordinarily high dose regions (1,000 mSv/h). The developed gamma camera is characterized by: (1) tolerance for high dose rate environments; (2) high spatial and spectral resolution for identifying unknown contaminating sources; and (3) good usability for being carried on a robot and remotely controlled. These are achieved by using a compact pixelated detector module with CdTe semiconductors, efficient shielding, and a fine resolution pinhole collimator. The gamma camera weighs less than 100 kg, and its field of view is an 8 m square in the case of a distance of 10 m and its image is divided into 256 (16 x 16) pixels. From the laboratory test, we found the energy resolution at the 662 keV photopeak was 2.3% FWHM, which is enough to identify the radionuclides. We found that the count rate per background dose rate was 220 cps h/mSv and the maximum count rate was 300 kcps, so the maximum dose rate of the environment where the gamma camera can be operated was calculated as 1,400 mSv/h. We investigated the reactor building of Unit 1 at the Fukushima Dai-ichi Nuclear Power Plant using the gamma camera and could identify the unknown contaminating source in the dose rate environment that was as high as 659 mSv/h.

Keywords: gamma camera; pinhole collimator; CdTe detector.

1. Introduction

The tsunami following the Great East Japan Earthquake on March 11, 2011 damaged power supply equipment that led to loss of cooling functions and eventually, the severe accident in the

Fukushima Dai-ichi Nuclear Power Plant (FDNPP), which resulted in the release of radioactive materials into the environment [1]. Radioactive contamination still remains inside and outside the power plant. To effectively perform decontamination work for restoration from the accident, it is necessary to identify the source positions. Gamma cameras which can visualize a radiation intensity distribution of a wide area in a short time are required, and some gamma cameras have been developed for this purpose. However, it has never been reported that a gamma camera was able to identify the positions of contaminants and radionuclides in the high dose environments where it was surrounded by a lot of radioactive contaminations.

The gamma cameras can be classified into three types: a pinhole type [2-4] and a coded aperture type [5-9], each of which has a collimator, and a Compton type camera [10-14] which does not need the collimator. Each type has different characteristics due to the different imaging principles. Recently, coded aperture cameras and Compton cameras have been developed. These are generally used because high sensitivities are possible and light weight can be realized with an appropriate configuration. It is generally recognized that the pinhole camera has the lowest sensitivity due to the pinhole collimator and is the heaviest due to the shield because scintillators with photomultipliers which are conventionally used in the pinhole camera increase size. However, the pinhole camera is the simplest, most robust and has the best quantitativity by employing enough shielding. If small detectors and circuits are loaded into the pinhole camera instead of scintillators and photomultipliers, the pinhole camera could be used in the high dose environments.

In order to use gamma cameras especially in high dose environments like FDNPP, gamma cameras must not only withstand the high dose rate environments, but also be light and stable enough to allow them to be carried on a robot and remotely controlled in the field. The pinhole camera has the best potential of the three types in this application because both its principle and structure are the simplest. By using the compact pixelated semiconductor detector module with new modified ASICs (Application-Specific Integrated Circuits) and making a fine resolution pinhole collimator with enough shielding, we have developed a pinhole gamma camera which satisfies the above mentioned requirements especially in the high dose environments.

In this paper, we present the results of performance tests of our original gamma camera.

2. Spectroscopic gamma camera system for high dose environments

2.1. Concept of the system

The developed gamma camera is characterized by: (1) tolerance for high dose rate environments; (2) high spatial and spectral resolution for identifying the unknown contaminating sources; and (3) good usability for being carried on a robot and remotely controlled. To carry out these features we

adopted the pinhole camera structure. The key components to determine the performances of the pinhole gamma cameras are a detector module, a pinhole collimator, and shielding structure.

The detector module is the most important component. It must be compact, have a high energy resolution, and withstand a high count rate. Then we adopted the semiconductor detector module we originally developed for nuclear medicine systems [15-17].

The pinhole collimator determines the image specifications (i.e. field of view and spatial resolution) and sensitivity. Roughly speaking, a trade-off needs to be found between spatial resolution and sensitivity. However, there are enough signals in the high dose environments, so we designed the pinhole collimator considering the spatial resolution preferentially.

The shielding structure determines tolerance for the high dose rate environments and the weight of the system. Gamma-rays passing through the shield generate background signals, which should be suppressed to carry out highly quantitative measurement and to keep background signal count rate well below the circuit limit (maximum count rate of the detector module). We determined the necessary shielding thickness by estimating the count rate to keep the system reasonably light in weight.

The performances of the gamma camera are determined compositely by the components as mentioned above. So we set design goals according to the three features, i.e. the gamma camera must: (1) withstand a maximum environmental dose rate of 1,000 mSv/h; (2) have a spatial resolution of less than 1.0 m at a distance of 10 m; and (3) weight less than 100 kg so it can be carried by a robot.

2.2. Compact pixelated semiconductor detector module

Our gamma camera has a compact pixelated semiconductor detector module (Fig. 1), which was originally developed for medical applications. With the semiconductor detectors, optical devices such as photomultiplier tubes are not needed, the detectors can be easily pixelated and have a high energy resolution.

The detector module has 256 (16 x 16) pixels of CdTe and ASICs for signal processing. The thickness of CdTe detectors is 5 mm, and the pixel pitch is 2.5 mm, corresponding to the module size of 40 mm square.

The CdTe detectors have high energy resolution and we had previously developed a low noise ASIC, so the gamma camera can precisely measure the energy of each incident photon. The gamma camera should therefore be able to identify radionuclides and their distribution. Furthermore, the band gap of CdTe is 1.44 eV, and the temperature dependence of the signal gain of CdTe is much less than that of the scintillators [18]. This means that the gamma camera can be used at room temperature inside and outside buildings.

The ASIC was originally developed for nuclear medicine systems, so the count rate performance

was not necessarily sufficient for measurements in the high dose environments. The detector module using the ASICs was saturated with the input gamma-rays of 250 kcps. To endure higher count rate, we re-designed the ASIC to have a reduced number of channels bound to one trigger from 16 to 8. By using the new ASICs, the gamma camera is expected to withstand double the count rate and to be used in the high dose environments inside FDNPP without an excessive weight increase.

2.3. Fine resolution pinhole collimator

Pinhole collimator configuration was determined to have the required field of view and spatial resolution. Assuming the gamma camera will be used inside a nuclear plant, we set an 8 m square FOV and a spatial resolution of less than 1 m at a distance of 10 m. With this FOV, the opening angle of the pinhole was calculated to be 59º and the distance r between the pinhole and detectors (see Fig. 2) to be 50 mm.

The diameter of the pinhole was set as 2 mm to achieve the required spatial resolution as derived below. In Fig. 2, b is the diameter of the pinhole, and r and R are the distances between detectors and the pinhole and between the pinhole and measuring objects, respectively. Spatial resolution X is derived geometrically as

$$X = b + bR/r. \quad (1)$$

We next derive an effective pinhole diameter. As Fig. 2 shows, the pinhole has a knife edge shape, and gamma-rays can be considered to pass through a shield of mean free path (μ^{-1}) thickness effectively. As the material of the pinhole collimator, we employed tungsten, which has a high volumic mass of 19.3 g/cm^3 and an atomic number of 73. So, the effective pinhole diameter B is

$$B = b + \mu^{-1} \tan(\alpha) \approx b + 3.0 \text{ mm}, \quad (2)$$

where μ^{-1} of Cs-137 (662 keV) in tungsten is 5.3 mm and α is 29.5º. Therefore, we obtain the spatial resolution shown in Fig. 3 from eq. (1). From Fig. 3, we set the pinhole diameter as 2 mm to achieve 1 m spatial resolution at a distance of 10 m.

2.4. Enough shielding for high background

Here we defined the target background dose rate at 1,000 mSv/h, and determined the necessary shielding thickness by estimating the background and signal count rate as follows to keep the system as light as possible.

We assume there is a Cs-137 point source of Q (MBq) at a distance of R (m), then effective dose rate E (μSv/h) is, $E = \Gamma Q/R^2$, where Γ (μSv m^2/MBq/h) is the 1 cm dose rate constant of Cs-137. Then, incident photon flux to the gamma camera F (counts/s/m^2) can be calculated as

$$F = QI/(4\pi R^2) = EI/(4\pi\Gamma), \quad (3)$$

where I corresponds to the emission rate of 662 keV gamma-rays. From eq. (3), the flux F corresponding to 1 mSv/h generated by Cs-137 is calculated as 0.73×10^5 (counts/s/cm^2), by using Γ

of 0.0927 (μSv m^2/MBq/h) and I of 0.851. If this flux is directly exposed on the CdTe detectors without any shield, the expected count rate is 2.3×10^5 (cps), where 0.2 and 16 (cm^2) correspond to quantum efficiency and area of CdTe detector, respectively. In other words, count rate per dose rate on the CdTe detector module is 230 kcps h/mSv. Here, we assume the radioactivity is uniformly distributed around the gamma camera. Because the effective pinhole diameter can be calculated as 5.0 mm from eq. (2), the solid angle ratio of the signal area (= pinhole aperture) to the background area is 6.2×10^{-4}. Then, the total count rate is,

$$(230\beta \times (1 - 6.2 \times 10^{-4}) + 230 \times 6.2 \times 10^{-4}) \text{ kcps h/mSv}, \quad (4)$$

where β is an attenuation factor of the shielding. In order to carry out the measurement under the environmental dose rate of 1,000 mSv/h with our new modified ASIC which is going to be saturated with the input count rate of 500 kcps, the condition of β can be derived as:

$$\beta < 1.6 \times 10^{-3}. \quad (5)$$

Then we employed tungsten of 27.5 mm thick as an inner shield and 20 mm lead as an outer shield, which meant the total β was 1×10^{-3}. We chose tungsten as the inner shield to reduce the weight, and total weight of the shielding is 55 kg.

2.5. Configuration of the system

A photo of the developed gamma camera is shown in Fig. 4, and its main specifications are listed in Table 1. As mentioned above, the gamma camera is a pinhole camera with the semiconductor detectors covered by 27.5 mm thick tungsten plus 20 mm thick lead shielding. The gamma camera is also equipped with an optical camera to obtain corresponding visible images, a scanning laser range finder, and a lead shutter. The total weight of the system is 80 kg.

The gamma camera can derive intensities of point sources (dose rates at a distance of 50 cm) by appropriately handling sensitivity variation among pixels, distances to the targets, and background. Variation of the sensitivity is caused by intrinsic differences among the detector pixels and by systematic differences of solid angles related to the incidence angles. This variation is corrected using a data table which is obtained by prior measurement. Since the gamma camera has the scanning laser range finder, it is able to measure distances to objects, and dose rate on each pixel can be calculated. It is easy to assume that background signals through the shield increase in the high dose environments, therefore background subtraction is necessary. Since the gamma camera has the lead shutter, the background signals are measured by covering the pinhole and the background data can be removed.

The control of the gamma camera, including data acquisition and data handling, is carried out with a laptop PC (designated the “control PC”) which is connected with the gamma camera through a USB cable. The measurement results calculated with the PC are displayed on the screen every second. Because it is desirable that the measurement tasks under the high dose environments are

performed without operators, the gamma camera is designed to be mounted on a robot. Fig. 5 shows a configuration for the investigations in the FDNPP. The control PC (not shown in Fig. 5), which is carried on the robot, is connected with the operating PC through the LAN. We can operate the gamma camera and confirm the results of measurements by displaying the control PC screen on the operating PC with a VNC (Virtual Network Computing) application.

3. Performance tests

We examined the performances of this gamma camera according to three key features described in section 2. In section 3.1, tolerance for the high dose rate environments was verified in a count rate performance test and a shield performance test. Energy resolution, spatial resolution and dose rate accuracy tests are also described. In section 3.2, three key features were verified through the survey in the FDNPP.

3.1. Laboratory test

A. Count rate performance test

We evaluated count rate performance of the gamma camera to confirm improvement of the modified ASIC. Because it is difficult to measure accurately the count rate performance with radionuclides such as Cs-137 or Cs-134, we used Tc-99m instead. Tc-99m is generally used in nuclear medicine diagnosis, and the energy of the gamma-rays is 140.5 keV and the half-life is 6 hours. We first measured the count rate with Tc-99m of about 1 GBq at a distance of 25 cm without the shielding. We continued to measure the count rate once an hour for three days, when the relative intensity became 1/4096, so we could ignore dead time (we could regard incident and output count rates to be equal).

The relationship of the output count rate versus the input count rate (Fig. 6) was determined by calculating input count rates in consideration of the Tc-99m decay in each measurement. For comparison, Fig. 6 also plots the result obtained with the old ASICs. The output count rate of the old ASICs reaches a maximum of 154 kcps when the input count rate becomes 300 kcps (dead time is 49%), and decreases above this point. The new ASICs show improvement; the output count rate is 249 kcps with the input rate of 300 kcps (dead time is 17%). Unlike the old ASICs, the output count rate shows a plateau at input count rates from 300 to 900 kcps. This is caused by a limit of the digital signal processing in the post stage (a communication bandwidth on the FPGA), which is a new bottleneck unexpected with the conventional circuits. The output count decreases above the input count rate of 900 kcps similar to the old ASIC. If there is no bottleneck, we can expect that the new

modified ASICs to achieve the maximum output rate at the input count rate of approximately 600 kcps assuming similar count rate performance to the old ASICs. This is twice as high a count rate as that of the old ones.

B. Shield performance test

In order to verify the maximal dose rate environment where the gamma camera can function, we put a Cs-137 point source (293 MBq) at various distances around the gamma camera (Fig. 7), and measured the count rate. Fig. 8 plots the count rates versus dose rates which are calculated at positions of the detector module from 1 cm dose rate constant of Cs-137. The maximum count rate per dose rate is 220 cps h/mSv, which occurs in the case of vertical incidence to the shielding. The obtained count rate is much lower when the Cs-137 is positioned at the left front of the gamma camera, due to the effective shielding caused by the oblique incidence.

As mentioned in section 2.4, if the detector is exposed to the radiation without shielding, the count rate per dose rate would be 230 kcps h/mSv. So, 220 cps h/mSv with the shielding corresponds to β value of 9.6×10^{-4}, and we confirm that the detector shielding functions as expected.

C. Energy resolution to identify nuclides

The energy spectrum summed over all the detectors (256 pixels), which was measured with a point source of Cs-137 without the pinhole collimator, is shown in Fig. 9. The energy resolution of the summed spectrum is as high as 2.3% FWHM at the 662 keV photopeak. The spectrum obtained for a soil sample contaminated by the Fukushima accident is also shown in Fig. 9. Photopeaks of 662 keV (Cs-137) and 605 keV (Cs-134) are clearly separated, thus we confirm the gamma camera can identify radionuclides.

D. Spatial resolution for use in nuclear power plants

Imaging capability is also verified. Fig. 10 shows a gamma camera image obtained with a Cs-137 point source at a distance of 5 m, overlaid on the optical image. The position of the point source obtained with the gamma-ray image and that with the optical image coincide well with each other. The gamma camera can therefore visualize the radioactive sources.

To evaluate spatial resolution, a one-dimensional count profile was derived from Fig. 10 (blue rectangular area), and it is shown in Fig. 11. The spatial resolution of the point spread function is 1.72 pixels FWHM, which corresponds to 4.9º. This can be converted into 0.86 m at a distance of 10 m. Thus we verify the designed imaging capability.

E. Dose rate accuracy

To check the accuracy of the dose rate measurement, we tested a Cs-137 point source (293 MBq)

at nine points located on a plane at a distance of 1.5 m and at one point of 5 m (see Fig. 12). For reference, the dose rate measured at a distance of 50 cm by a dosimeter is 110 μSv/h, which is consistent with the value of 109 μSv/h calculated from the 1 cm dose rate constant of Cs-137 (0.0927 μSv m^2/MBq/h). Fig. 13 shows the result. Measurement errors from the reference (110 μSv/h) are within 5%.

3.2. Radioactive contaminates survey in the FDNPP

In December 2013, we investigated the Unit 1 reactor building at the FDNPP using our gamma camera. As shown in Fig. 5 and Fig. 14, we carried out the investigation by remotely operating the gamma camera on a robot. Fig. 15 shows measurement points of the south side of the Unit 1 reactor building where measurement with conventional gamma cameras is challenging because of the extremely high dose rate. We measured all directions at points 1 and 2, and measured hot spots at point 3. To fully cover a hemisphere with the gamma camera FOV of 44º (= $2\tan^{-1}(4/10)$), we set 12 directions with the elevation angles of 10º and 50º, and 1 direction with the angle of 90º, so eventually 25 measurements were carried out in each point. Exposure times of the normal and background measurements were both 15 s.

Table 2 presents dose rates, average and maximum count rates of the gamma camera at each measurement point. The dose rate was the highest at point 3, and even in this environment the observed maximum count rate was 122 kcps (< 249 kcps) and the gamma camera was not saturated.

An energy spectrum summed over all directions at point 1 is shown in Fig. 16. The count ratio of the Cs-134 photo peaks (796 and 802 keV) to the Cs-137 photo peak (662 keV) after subtraction of continuum components (Fig. 16) was 0.37. To obtain the ratio of Cs-134 to Cs-137 radioactivity at the time of the nuclear accident, we have to consider branching ratios, decays, effective pinhole diameters, and detection efficiencies. As a result, we obtain the value of 0.95, which was consistent with the generally considered ratio of 1.0 [19-20]. It is not necessary to separate Cs-134 and Cs-137 hot spots, but this result shows that we can actually distinguish plural nuclides and evaluate relative radioactivity between plural nuclides by using the gamma camera.

The images obtained at points 2 and 3 are shown in Fig. 17 and Fig. 18, respectively. In some of the images, a pipe running in the ceiling is depicted in red, but there are no high dose areas in other images; therefore, we attribute the high dose rate in this region to this pipe.

4. Discussion

We have developed the gamma camera in order to measure distributions of radioactive material

contaminants and to identify radionuclides in extraordinarily high dose regions (1,000 mSv/h). From the results of the count rate performance test and the shielding performance test, the maximum input count rate without saturation is 300 kcps and the count rate per dose rate is 220 cps h/mSv, then the maximum dose rate of the environment where the gamma camera can operate is calculated as 1.4 Sv/h. However, we measured the count rate performance by using Tc-99m, so differences between Tc-99m and Cs-134 or Cs-137 have to be considered. Because of an increase of Compton scattering events, there may be more simultaneous events within an ASIC in the case of Cs-134 or Cs-137 than Tc-99m. Then slope of a count rate performance curve of Cs-134 or Cs-137 may be smaller than that of Tc-99m On the other hand, the saturation of the output count rate is caused by a limit of the digital signal processing in the post stage, so saturation output count rate of Cs-134 or Cs-137 may be the same as Tc-99m. Therefore, output count rates may be saturated at 249 kcps with input count rates over 300 kcps and under 900 kcps. This means that in high dose environments we can use the gamma camera without saturation under a dose rate of at least 1.4 Sv/h. These results also show problems that errors of evaluated dose rates increase when output count rates become close to 249 kcps because of the increase of the signal processing dead time, and evaluated dose rates are not correct when output count rates exceed 249 kcps especially. To improve quantitativity in high dose environments, it is necessary to remove the bottleneck of the digital signal processing, and to estimate a count rate performance curve of Cs-134 or Cs-137 by simulations instead of measuring actual radionuclides.

If we can resolve the bottleneck, we expect that the maximum input rate will increase to over 600 kcps. This means that the improved gamma camera will be able to be used in approximately twice as high a dose rate area, that is, at least 2.8 Sv/h. Furthermore, because we have not optimized the thickness of CdTe detectors which had been developed for the medical use, by adopting thinner CdTe detectors the maximum environment dose rate will be increased to more than 2.8 Sv/h.

We investigated the Unit 1 reactor building of FDNPP using the gamma camera. The highest dose rate was 659 mSv/h, and the gamma camera could operate without saturation and identify the radiation source of a high dose area. From the results of laboratory tests, we calculated that the input count rate would be 150 kcps at the dose rate of 659 mSv/h, and the output count rate would be 140 kcps from Fig. 6. The maximum and average output count rates actually measured were 122 kcps and 81.4 kcps, respectively. The lower values than the expected would be explained by the shielding performance test conditions of the minimum shielding direction and by the difference of Tc-99m and Cs as mentioned above.

5. Conclusion

We have developed a gamma camera that has three key features: (1) tolerance for the high dose rate environments; (2) high spatial and spectral resolution; and (3) good usability. By using the compact semiconductor detector module with the modified ASICs to endure higher count rate and by designing enough shielding, we broke through the trade-off between weight increase with enough shielding for feature (1) and light weight structure for feature (3). The developed gamma camera has high spatial resolution and high energy resolution by using a finely pixilated semiconductor detector module and making a fine resolution pinhole collimator. These basic specifications were evaluated in laboratory tests. Finally, we investigated the Unit 1 reactor building of FDNPP with the gamma camera on a robot, and we could remotely identify the unknown contaminating source in the high dose rate environment of 659 mSv/h.

Acknowledgment

This work was supported in part by New Energy and Industrial Technology Development Organization. Also, this work includes the results of the project subsidized by the Ministry of Economy, Trade and Industry and the project undertaken by Hitachi-GE Nuclear Energy, Ltd. as a member of the International Research Institute for Nuclear Decommissioning.

References

[1] T.J. Yasunari, A. Stohl, R.S. Hayano, J.F. Burkhart, S. Eckhardt, and T. Yasunari, “Cesium-137 deposition and contamination of Japanese soils due to the Fukushima nuclear accident,” Proc. Nat. Acad. Sci. U.S.A., vol. 108, pp. 19530-19533, 2011.

[2] O. Gal, F. Jean, F. Lainé, and C. Lévêque, “The CARTOGAM portable gamma imaging system,” IEEE Trans. Nucl. Sci., vol. 47, pp. 952-956, June 2000.

[3] O. Gal, B. Dessus, F. Jean, F. Lainé, and C. Lévêque, “Operation of the CARTOGAM portable gamma camera in a photon-counting mode,” IEEE Trans. Nucl. Sci., vol. 48, no. 4, pp. 1198-1204, Aug. 2001.

[4] S. Yamamoto, H. Watabe, N. Kawachi, S. Fujimaki, K. Kato, and J. Hatazawa, “Three-layer GSO depth-of-interaction detector for high-energy gamma camera,” Nucl. Instr. Meth. in Phys. Res. A, vol. 743, pp. 124-129, 2014.

[5] M. Woodring, D. Beddingfield, D. Souza, G. Entine, M. Squillante, J. Christian, A. Kogan, "Advanced multi-dimensional imaging of gamma ray radiation," Nucl. Instr. Meth. in Phys. Res. A, vol. 505, pp. 415-419, 2003.

[6] M. Gmar, O. Gal, C. Le Goaller, O. P. Ivanov, V. N. Potapov, V. E. Stepanov, F. Lainé, and F.

Lamadie, “Development of Coded-Aperture Imaging With a Compact Gamma Camera,” IEEE Trans. Nucl. Sci., vol. 51, no. 4, pp. 1682-1687, Aug 2004.

[7] F. Carrel, R. A. Khalil, P. Blot, K. Boudergui, S. Colas, M. Gmar, F. Lemasle, N. Saurel, V. Shoepff, H. Toubon, “GAMPIX: a new generation of gamma camera for hot spot localisation,” ISOE Proceedings, Cambridge, November 2010.

[8] F. Carrel, R. A. Khalil, S. Colas, D. de Toro, G. Ferrand, E. Gaillard-Lecanu, M. Gmar, D. Hameau, S. Jahan, F. Laine, A. –S. Lalleman, F. Lemasle, C. Mahe, J. –E. Maurer, N. Menaa, S. Normand, H. Onillon, N. Saurel, “GAMPIX: a New Gamma Imaging System for Radiological Safety and Homeland Security Purposes,” IEEE NSS/MIC, pp. 4739-4744, 2011.

[9] H. Lemaire, R. Khalil, K. Amgarou, J. Angélique, F. Bonnet, D. Toro, F. Carrel, O. Giarmana, M. Gmar, N. Menaa, Y. Menesguen, S. Normand, A. Patoz, V. Schoepff, P. Talent, and T. Timi, “Implementation of an imaging spectrometer for localization and identification of radioactive sources,” Nucl. Instr. Meth. in Phys. Res. A, vol. 763, pp. 97-103, Nov 2014.

[10] F. Zhang, Z. He, “New Readout Electronics for 3-D Position Sensitive CdZnTe/HgI_2 Detector Arrays,” IEEE Trans. Nucl. Sci. vol. 53, pp. 3021-3027, 2006.

[11] S. Takeda, H. Aono, S. Okuyama, S. Ishikawa, H. Odaka, S. Watanabe, M. Kokubun, T. Takahashi, K. Nakazawa, H. TajimaHiro, and N. Kawachi, “Experimental results of the gamma-ray imaging capability with a Si/CdTe semiconductor Compton camera,” IEEE Trans. Nucl. Sci., vol. 56, no. 3, pp. 783-790, 2009.

[12] H. Odaka, Y. Ichinohe, S. Takeda, T. Fukuyama, K. Hagino, S. Saitou, T. Sato, G. Sato, S. Watanabe, M. Kokubun, T. Takahashi, M. Yamaguchi, T. Tanaka, H. Tajima, K. Nakazawa, and Y. Fukazawa, “High-resolution Compton cameras based on Si/CdTe double-sided strip detectors,” Nucl. Instr. Meth. in Phys. Res. A, vol. 695, pp. 179-183, 2012.

[13] T. Takahashi, S. Takeda, S. Watanabe, and H. Tajima, “Visualization of Radioactive Substances with a Si/CdTe Compton Camera,” IEEE NSS/MIC, pp. 4199-4204, 2012.

[14] C. G. Wahl, W.R. Kaye, W. Wang, F. Zhang, J. M. Jaworski, A. King, Y. A. Boucher, Z. He, “The Polaris-H imaging spectrometer, ” Nucl. Instr. Meth. in Phys. Res. A, vol. 784, pp. 377–381, 2015.

[15] Y. Ueno, Y. Morimoto, K. Tsuchiya, N. Yanagita, S. Kojima, T. Ishitsu, H. Kitaguchi, N. Kubo, S. Zhao, N. Tamaki, and K. Amemiya, "Basic physical performances of a PET scanner using semiconductor detectors," IEEE Trans. Nucl. Sci., vol. 56, pp. 24-28, 2009.

[16] K. Tsuchiya, I. Takahashi, T. Kawaguchi, K. Yokoi, Y. Morimoto, T. Ishitsu, A. Suzuki, Y. Ueno, and K. Kobashi, “Basic performance and stability of a CdTe solid-state detector panel,” Ann. of Nucl. Med., vol. 24, No. 4, pp. 301-311, 2010.

[17] Y. Morimoto, Y. Ueno, W. Takeuchi, S. Kojima, K. Matsuzaki, T. Ishitsu, K. Umegaki, Y. Kiyanagi, N. Kubo, C. Katoh, T. Shiga, H. Shirato, and N. Tamaki, “Development of a 3D Brain

PET Scanner using CdTe Semiconductor Detectors and its First Clinical Application," IEEE Trans. Nuc. Sci., vol. 58, No. 5, pp. 2181-2189, 2011.

[18] T. Seino, and I. Takahashi, "CdTe Detector Characteristics At 30°C and 35°C When Using The Periodic Bias Reset Technique," IEEE Trans. Nuc. Sci., vol. 5, pp. 777-781, 2007.

[19] M. Komori, K. Shozugawa, N. Nogawa and M. Matsuo, "Evaluation of Radioactive Contamination Caused by Each Plant of Fukushima Daiichi Nuclear Power Station Using 134Cs/137Cs Activity Ratio as an Index," Bunseki Kagaku, vol. 62, No. 6, pp. 475-483 2013.

[20] K. Tagami, S. Uchida, Y. Uchihori, N. Ishii, H. Kitamura, and Y. Shirakawa, "Specific activity and activity ratios of radionuclides in soil collected about 20 km from the Fukushima Daiichi Nuclear Power Plant: Radionuclide release to the south and southwest," Science of the Total Environment, vol. 409, pp. 4885-4888, 2011.

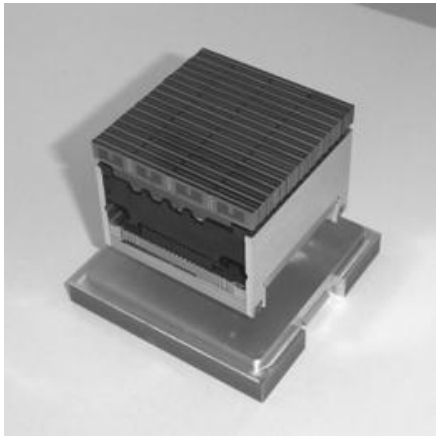

Fig. 1. CdTe semiconductor detector module.

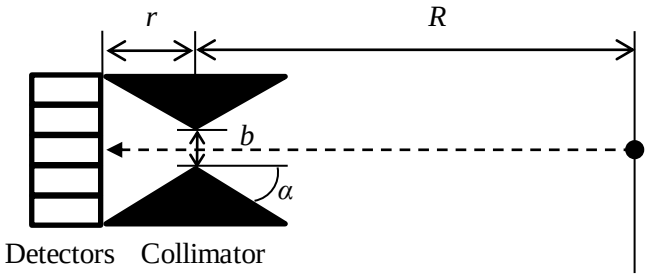

Fig. 2. Schematic of a pinhole collimator.

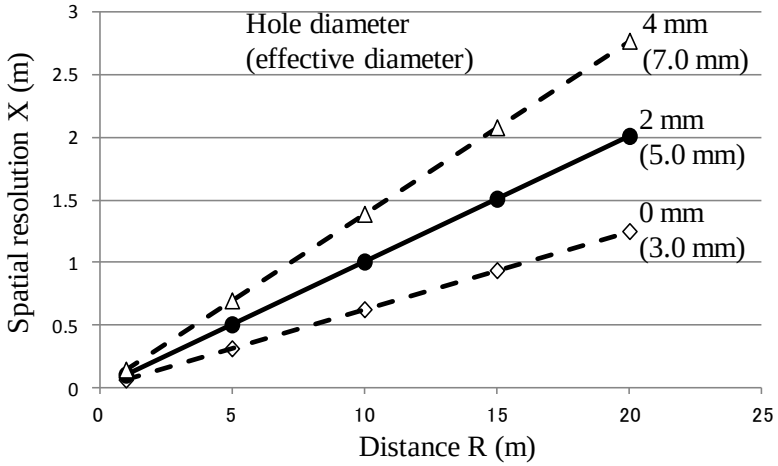

Fig. 3. Distance dependences of spatial resolution.

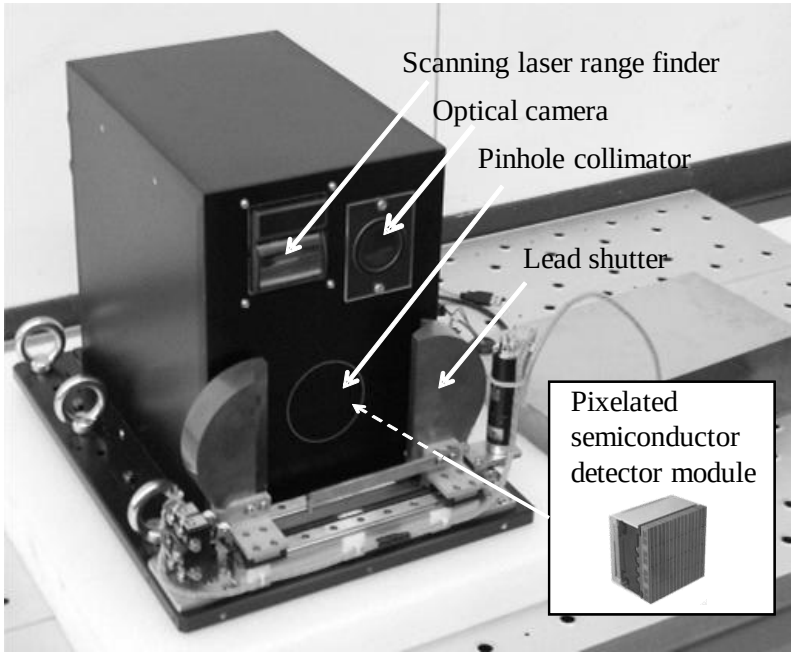

Fig. 4. Photo of the gamma camera.

Table 1. Specifications of the developed gamma camera

	Specs
Size	34 cm (W) x 43 cm (D) x 33 cm (H)
Weight	80 kg
Field of view	59° (= 8 x 8 m at 10 m)
Shielding	27.5 mm of tungsten and 20 mm of lead
Energy range	300 to 1,500 keV
Semiconductor detector module	CdTe (5mm thickness), 16 x 16 pixels
Pinhole collimator	Material: tungsten, pinhole diameter: 2mm

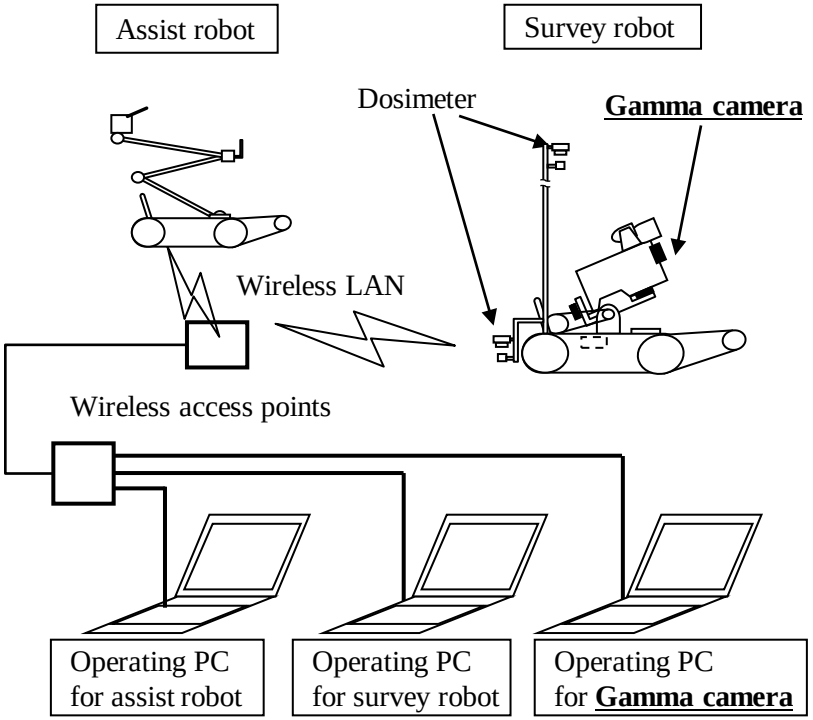

Fig. 5. Configuration for investigation. The gamma camera and Dosimeters are loaded on the survey robot and both are remotely controlled through the assist robot using PCs.

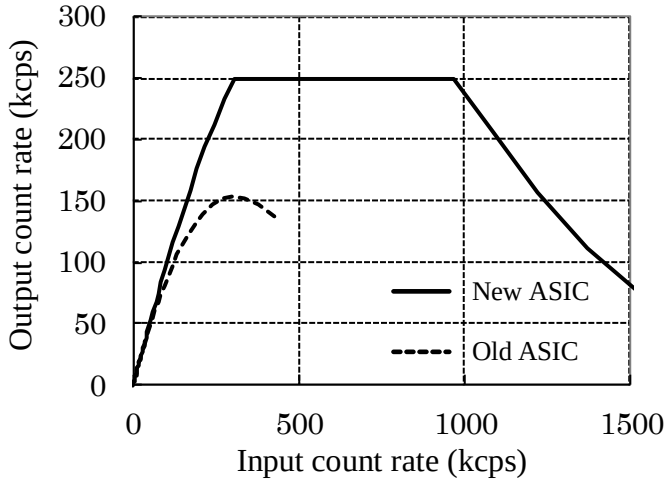

Fig. 6. Count rate performances of new and old ASICs.

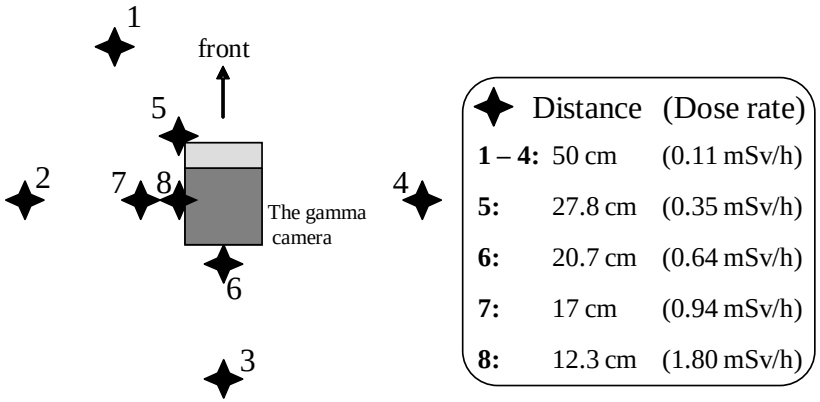

Fig. 7. Positions of a Cs-137 point source (293 MBq) in shielding performance test. Dose rates shown in the right panel were calculated from 1 cm dose rate constant of Cs-137 (0.0927 μSv m2/MBq/h).

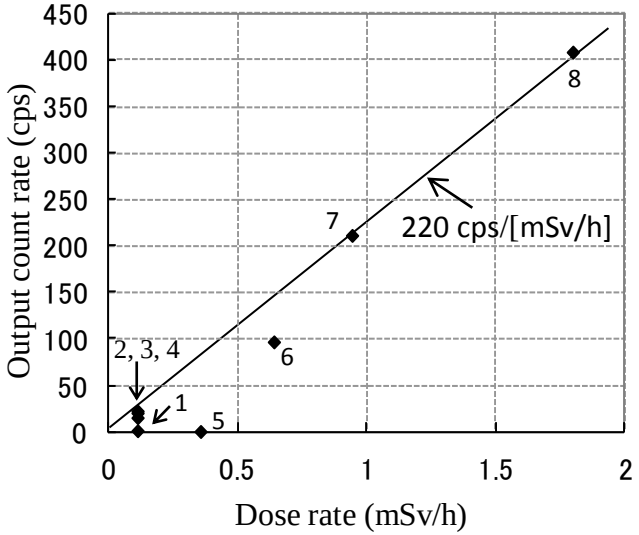

Fig. 8. Dose rate dependences of count rate.

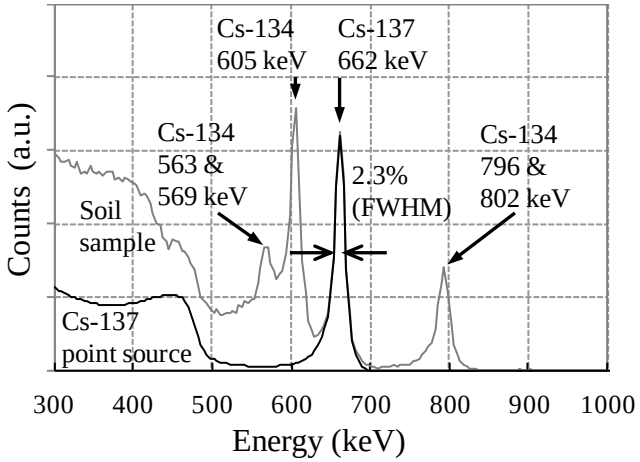

Fig. 9. Energy spectrums measured with a Cs-137 point source and a soil sample contaminated by the Fukushima Nuclear Power Plant accident.

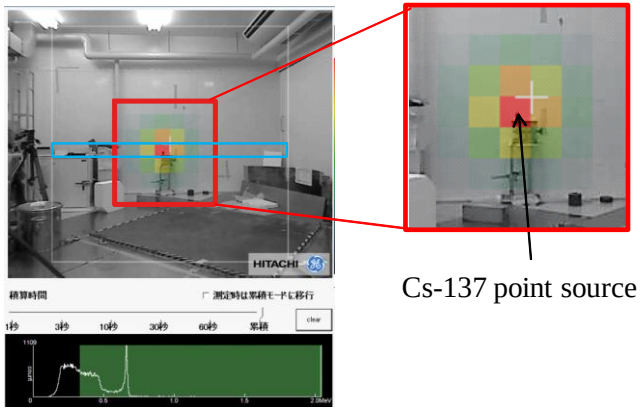

Fig.10. The gamma camera image obtained with a Cs-137 point source at a distance of 5m.

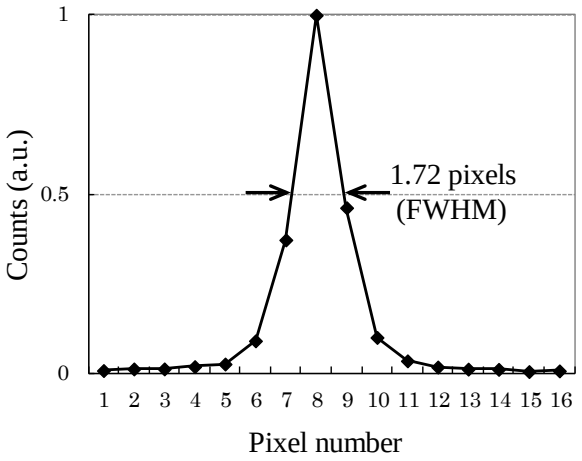

Fig. 11. Counts profile in blue square area of Fig. 10.

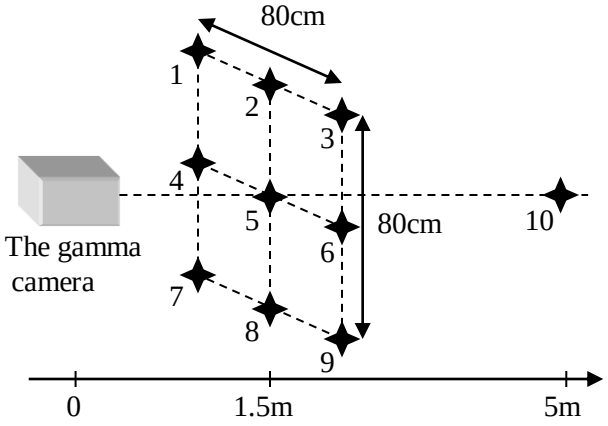

Fig. 12. Schematic view of dose rate accuracy test.

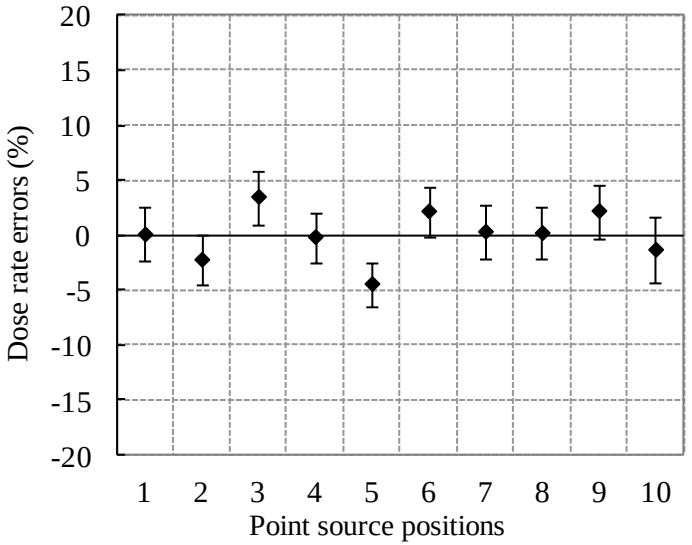

Fig. 13. Dose rate accuracy of each point in Fig. 12. Error bars denote statistical errors.

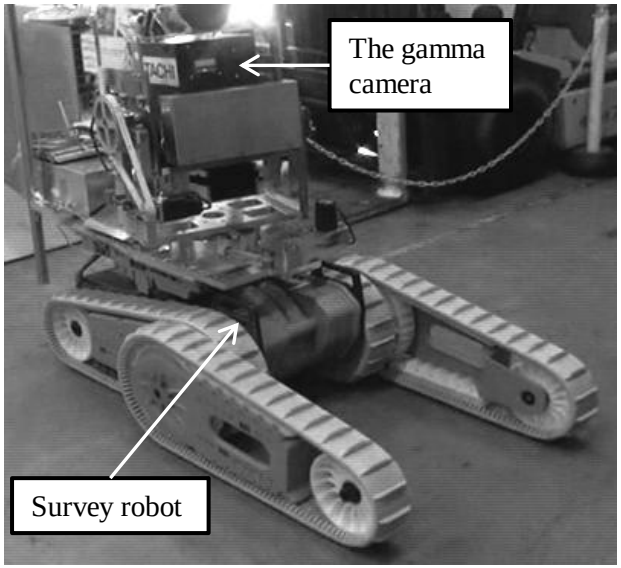

Fig. 14. Photo of the gamma camera loaded on the survey robot.

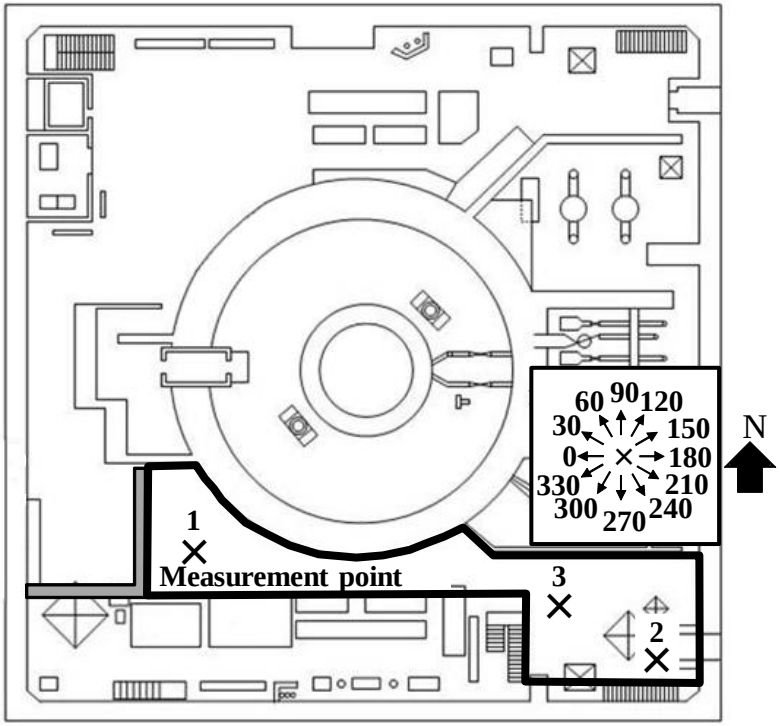

Fig. 15. Measurement points on the south side of the Unit 1 reactor building in FDNPP.

Table 2. Dose rate and count rate at each measurement point

Measurement point	Dose rate (mSv/h)	Ave. count rate (kcps)	Max. count rate (kcps)
1	13.0	2.2	14.5
2	167	15.0	66.8
3	659	81.4	122

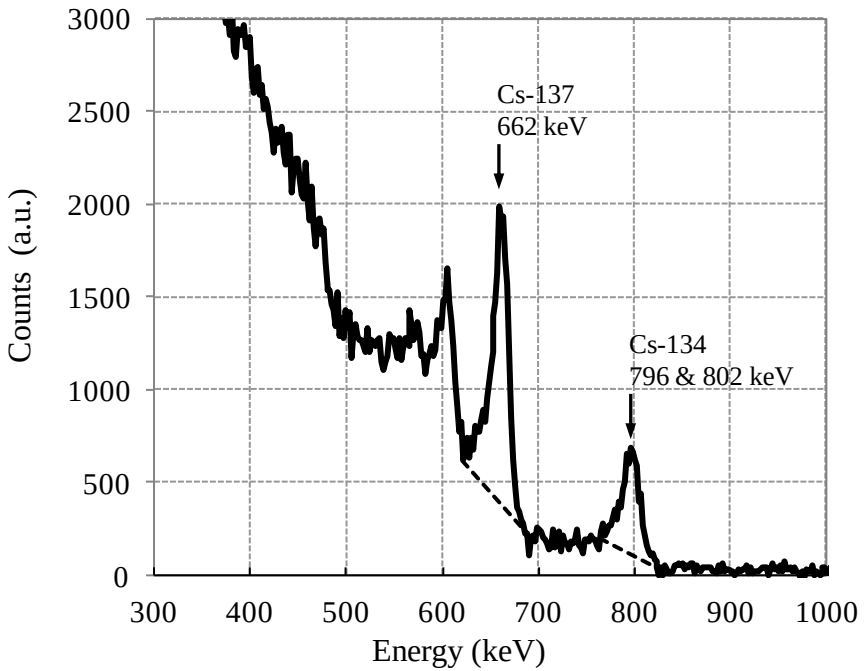

Fig. 16. Energy spectrum summed over all directions at point 1. The background was subtracted. Dashed lines represent continuum components in the analysis of count ratio.

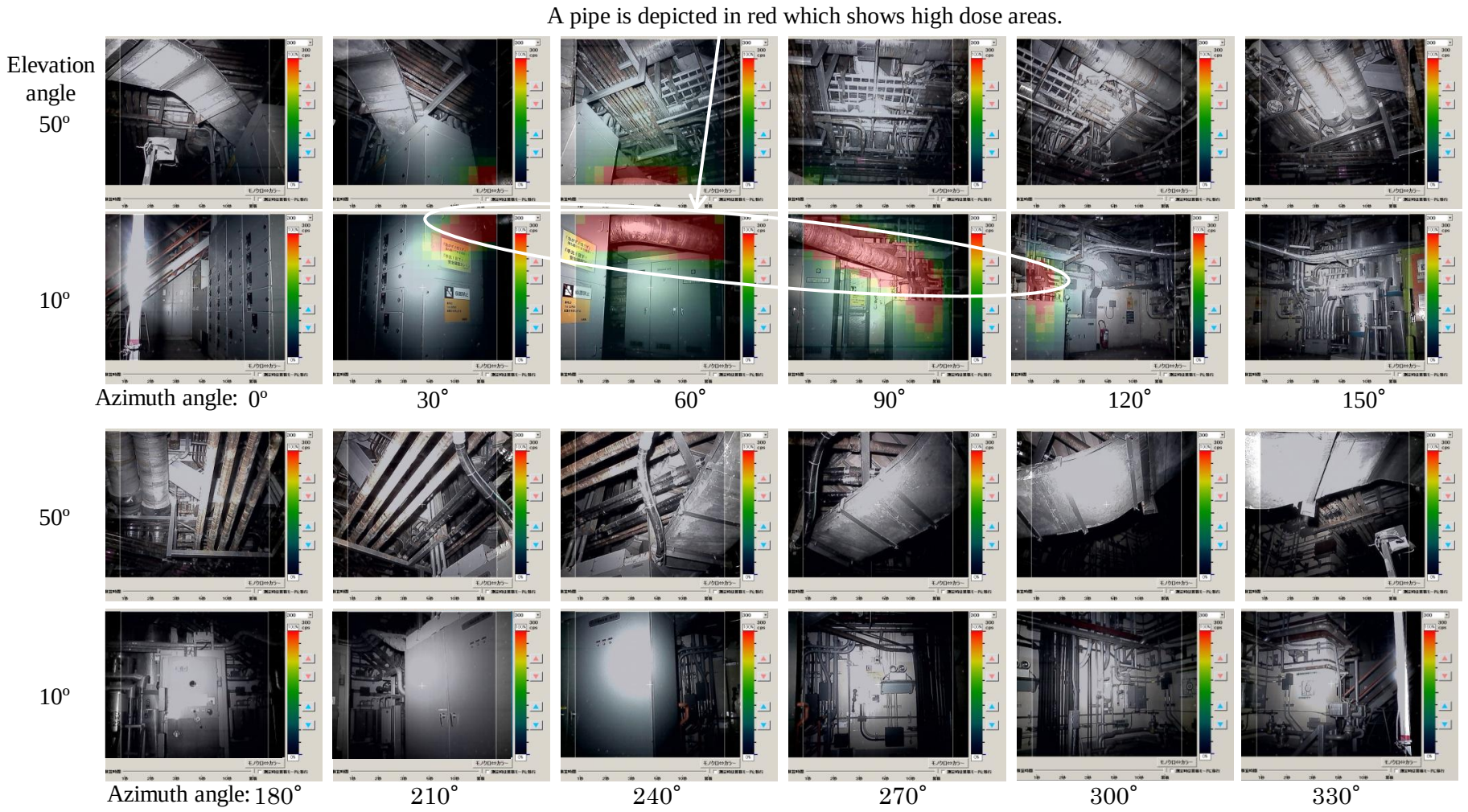

Fig. 17. Gamma camera images obtained at point 2.

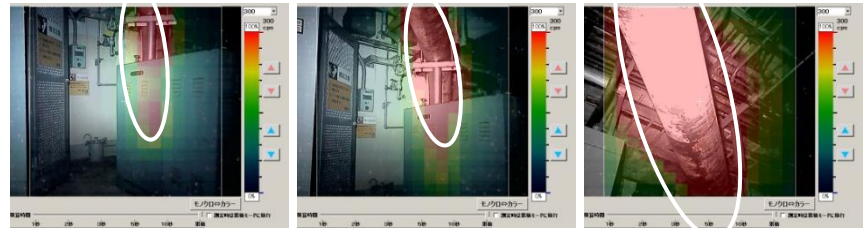

Fig. 18. Gamma camera images obtained at point 3.